INTERNATIONAL JOURNAL FOR NUMERICAL METHODS IN FLUIDS, VOL. 4, 231–246 (1984)

SIMULATIONS OF FLOWS AND WATER DEPTH IN A DENDRITIC RIVER SYSTEM

G. T. YEH

Environmental Sciences Division, Oak Ridge National Laboratory, Oak Ridge, Tennessee 37830, *U.S.A.*

SUMMARY

This paper presents the development of a channel hydrodynamic model for simulating the behaviour of flows and water depths in a river network that may consist of any number of joined and branched rivers/streams, including both tidal and non-tidal rivers. The model employs a numerical method—an integrated compartment method (ICM). The method greatly facilitates the set-up of algebraic equations for the discrete field approximating the corresponding continuous field.

Most of the possible boundary conditions that may be anticipated in real-world problems are considered. These include junctions, prescribed flow, prescribed water depth (or cross-sectional area), and rating curve boundaries. The use of ICM makes the implementation of these four types of boundary conditions relatively easy.

The model is applied to two case studies: first to a single river and then to a network of five river branches in a watershed. Results indicate that the model can simulate the behaviour of the hydrodynamic variables that are required to compute chemical transport in a river-stream network.

KEY WORDS Channel Flow River Modelling Integrated Compartment Method

INTRODUCTION

One of the critical issues involving existing chemicals and new chemical production is the safe use of potentially hazardous materials. Comprehensive assessments are needed to quantify the effects of chemical releases into the environment. Assessments would inevitably include transport, transformation, fate and pathway of the chemicals. They would also be concerned with exposure and the resulting health and ecological effects.

Environmental releases of chemicals may occur to aquifers, surface water regimes, oceans/estuaries, the atmosphere, or even directly to biota. However, following the release, there will be redistribution of the chemical(s) into all media. One of the important pathways of the chemicals from source release will be the stream/river network. The ability to simulate flow dynamics and water depth as functions of system parameters and of space and time is a prerequisite to the analysis of chemical transport, transfer, and transformation in the stream/river network. This paper presents the development of a channel hydrodynamic model that computes flow rates, water depth, cross-sectional areas, top width, and wet perimeter as function of time and longitudinal distance along the river/stream system. These variables provide the advection and dispersion mechanisms for the companion transport model of sediments and chemicals.[1] Existing literature and practical computer codes that deal with the stream/river network have almost exclusively used the kinematic approach.[2–4] The limitation of the kinematic approach is its inability to handle tidal rivers and backwater effects.[5,6] On the other hand, numerous reports are available that employ dynamic approaches to handle general transient flow conditions.[7–13] but most of these are limited to

0271–2091/84/030231–16$01.60
© 1984 by John Wiley & Sons, Ltd.
Received 24 June 1982
Revised 17 November 1982

single rivers or streams. The investigation of river networks with dynamic approaches has received great attention only since the early 1970s.[14–19] Wood *et al*[18,19] employed the method of characteristics to solve the full set of the Saint-Venant equations. The external boundary nodes and internal junctions were treated separately from the internal nodes by iterating the solution for interior nodes and that for the boundary nodes and junctions. Fread[8,16] treated the dendritic river system as consisting of a main steam and tributaries. An implicit finite difference scheme was used to solve for the complete set of dynamic equations for the main stem and tributaries separately. Iteration procedures were used until a correct lateral inflow from the tributaries to the main stem was obtained. Akan and Yen[14] presented a diffusion wave model to simulate unsteady flow in a dendritic network accounting for the downstream backwater effect by an overlapping technique.

The present model is developed to enable the dynamic simulation of flows and water depth in a network of rivers and streams. The basic complete set of governing equations for flow rates and water depth derived from three-dimensional Reynolds-averaged Navier–Stokes equations is adapted. The governing equations included an additional term to Saint-Venant equations[20] to account for turbulence and cross-sectional velocity shear. A minimum of approximations and assumptions are made. An integrated compartment method (ICM),[21] which is an extension of the integrated finite difference method (IFDM),[22] is used to simulate the behaviour of the set of governing equations. In this method, the link matrices are derived based on the fluxes of mass and momentum along each of the links that intertwine the compartments of the river system. The global matrix is then assembled from link matrices. The junctions and interior nodes on all branches are treated simultaneously.

MATHEMATICAL FORMULATION

Most of the derivations of the governing equations for channel flow dynamics start with a small control volume between two channel cross-sections at a distance of Δx as shown in Figure 1.[9,23] The conservation principles of mass, Q, and momentum, M, are then applied to

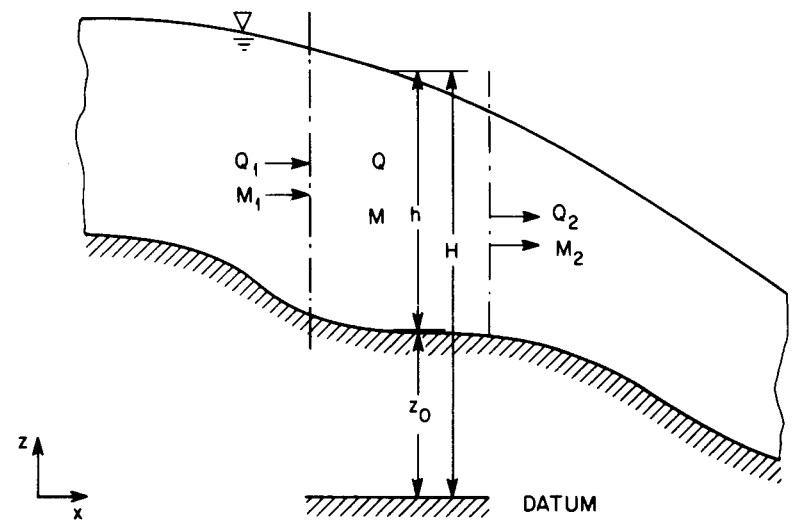

Figure 1. Control volume for deriving channel equations

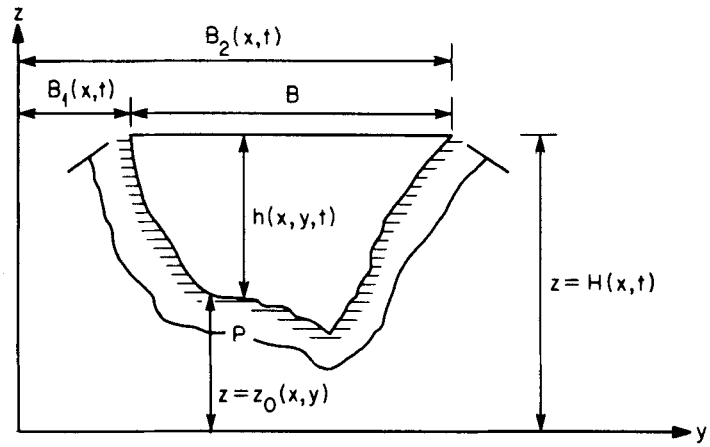

Figure 2. Channel cross-section

this slice of control volume. With this approach, many assumptions are lost, and boundary conditions on the transverse and vertical directions are not stated in the process of derivation. Instead, a general set of one-dimensional equations of continuity and momentum was derived by integrating the three-dimensional Reynolds-averaged Navier–Stokes equations over a cross-sectional area (Figure 2) to yield the following:[24]

$$\frac{\partial A}{\partial t}+\frac{\partial UA}{\partial x}=q \tag{1}$$

$$\frac{\partial Q}{\partial t}+\frac{\partial UQ}{\partial x}=-gA\frac{\partial h}{\partial x}-gA\frac{\partial z_0}{\partial x}+\frac{1}{\rho}(\tau^{w}B-\tau^{b}P)+\nu_{T}\frac{\partial^2 Q}{\partial x^2}+m/\rho \tag{2}$$

In equations (1) and (2), x is the longitudinal co-ordinate along the flow direction; t is the time; A is the cross-sectional area; Q is the flow rate; U is the average velocity given by $U = Q/A$; q is the source of lateral inflow per unit length that may result from precipitation on the river surface, surface runoff from land surface and seepage from groundwater; g is the gravitational acceleration; h is the water depth; z_0 is the elevation of the river bottom; ρ is the water density; m is the sum of the internal and external momentum sources per unit x-length; τ^{w} is the wind stress exerted on the water surface; B is the width of the surface; τ^{b} is the bottom shear stress; P is the wet perimeter and ν_{T} is the sum of eddy and dispersive viscosities.

It should be noted that equation (2) differs from the Saint-Venant equations in that an additional term, $\nu_{T}\partial^2 Q/\partial x^2$, is included to account for turbulent momentum transfer and cross-sectional velocity shear. This term results from the cross-sectional integration of the three-dimensional Reynolds-averaged Navier–Stokes equations and is mainly due to the inhomogeneous flow velocity over the cross-section associated with the advection terms. In spite of the nebulous circumstances, the inclusion of this term has several attractive properties. It allows for internal friction and thereby energy dissipation; it does represent actual physical processes (although not necessary accurate); and it is particularly suitable for damping short wave noises generated by numerical methods. It is further noted that both h and z_0 in equation (2) are functions of x, y and t; the sum of h and z_0 is a function of x and t only. Hence to get rid of the dependence of equation (2) on the co-ordinate y, h from here

on will be taken as the deepest depth at any cross-section and z_0 as the corresponding bottom elevation.

In equation (2), the two unknowns, τ^w and τ^b, are introduced as a result of cross-sectional integration. These two terms arise from the evaluation of the deviatoric stress tensor at the surface and the wet perimeter, respectively.

Thus, the number of unknowns exceeds the number of equations for our problem. To tackle this problem, we reviewed the frequently used empirical relations for τ^w and τ^b to establish a set of constitutive equations. It has been shown that under turbulent conditions, a quadratic bottom frictional law adequately represents the damping due to shear stress at the water–solid boundaries[25] Several similar empirical expressions—Manning, Chezy, and Darcy–Weisbach equations[26]—were originally derived from measurements of steady flow in channels or pipes. They have been used successfully in transient studies.[7–19] Those relationships are

$$\tau^b = \rho C_f U^2 \tag{3}$$

and

$$C_f = \begin{cases} \frac{1}{8} f_{DW} & (4a) \\ \dfrac{g}{C^2} & (4b) \\ \dfrac{n^2 q}{R^{1/3}} & (4c) \end{cases}$$

where f_{DW}, C, n, and R are the Darcy–Weisbach coefficients, the Chezy coefficient, the Manning roughness length, and the hydraulic radius, respectively. In this paper, the Manning formulation [that is equation (4c)] is used to compute the bottom frictional force, since it has been proven and well accepted in the engineering community.[27]

The wind stress on the surface, τ^w, is more complicated to handle because the water surface is deformable and the length scale of the turbulent wind field is large. Thus, the wind stress is highly variable in time and space. Several investigators[28–30] derived expressions for the average wind stress from measurements in the field. Those expressions can be given by the following equation:

$$\tau^w = \rho_a C_d W_{10}^2 \tag{5}$$

where ρ_a is the air density, W_{10} is the wind speed at 10 m above the surface and C_d is the wind drag coefficient. The value of C_d has been found to vary from approximately 0·001 upwards, according to various investigators.[28–31]

Initial and boundary conditions

Equations (1) and (2) and the channel geometry constitute the governing equations for the two dependent variables, Q and A. The geometry is characterized by the relationships between the cross-sectional area A and the water depth h, the water surface width B, and the wet perimeter P. To completely describe the physical system, initial and boundary conditions on Q and A must be provided. For any transient simulation, it will be assumed that Q and A are prescribed initially. They can be obtained either from field data or by simulating the steady-state version of equations (1) and (2). Both options are provided in this paper. The provision of prescribing the initial condition with steady state solution under time-invariant boundary conditions is particularly useful, since in many cases of field problems, initial values of Q and A are not explicitly available.

Four types of boundary conditions are considered in this paper. They arise mainly from physical considerations of most possible, real-world problems. These are: (i) prescribed flow Q, (ii) prescribed water depth h or the cross-sectional area A, (iii) prescribed functional relationship between flow and water elevation, and (iv) the junction of river branches. Conditions (i)–(iii) can be readily written in mathematical terms as follows:

$$Q = Q_g(t) \tag{6}$$

$$A = A_g(t) \tag{7}$$

and

$$Q = f(A) \tag{8}$$

where Q_g, A_g, and f are given flow rates, the given cross-section area, and the prescribed function, respectively. Condition (iv) may be obtained by the principle of conservation of mass. Considering a junction as shown in Figure 3, the continuity of water flow may be written as:

$$\frac{dV_J}{dt} = Q_1 + Q_2 - Q_3 \tag{9}$$

where V_J is the volume of the junction and Q_1, Q_2, and Q_3 are the flow rates from river branches 1, 2, and 3, respectively. However, the values of Q_1, Q_2, and Q_3 depend on the water elevation at the junction J as well as on their respective branch conditions. To uniquely define the problem, a relationship between the volume V_J and its water depth h_J will be assumed to be describable. Written in mathematical terms, it is

$$V_J = f_J(h_J) \tag{10}$$

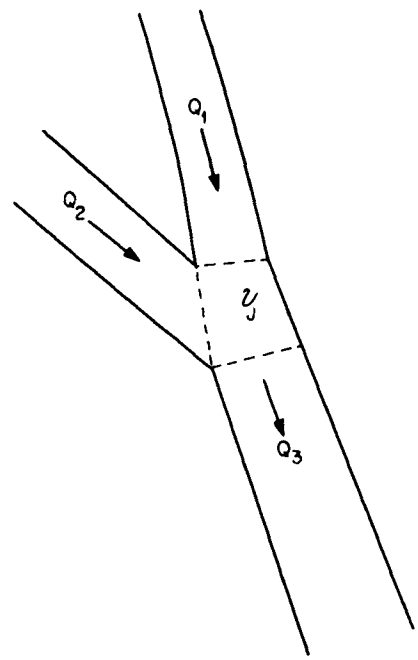

Figure 3. Channel junction

Equations (6)–(10) basically cover all the boundary conditions that may be anticipated in simulating the flow rate and water depth in any branched and joined river system. For example, equation (6) is normally applied to the upstream end, equation (7) to the downstream end, equation (8) to a weir or dam, and equations (9) and (10) to the place where two or more comparably sized rivers meet. The boundary condition of prescribed water depth is, in general, applied to the outlet of the river, since water is usually discharged into large water bodies where the water elevation is normally recorded.

NUMERICAL ALGORITHM

Analytical solutions of equations (1) and (2) under boundary conditions [equations (6)–(8)] do not exist for general problems. Numerical methods are thus needed to simulate the behaviour of the system. An integrated compartment method (ICM)[21] will be used for solving equations (1) and (2).

As an example, a one-dimensional compartment i with length Δx_i will be considered. It may be joined on either of its ends by a compartment j with length Δx_j as shown in Figure 4.

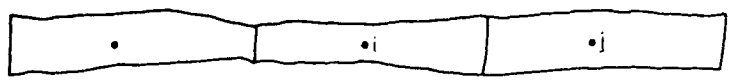

Figure 4. Compartments and links

Applying the principle of ICM to equation (1), we obtain the following equation for the discrete value of cross-sectional area A_i at compartment i:

$$\frac{dA_i}{dt}\Delta x_i = -\sum_{j\in N_i}(n_{ij}\,.\,U_{ij})A_{ij} + q_i\,\Delta x_i \tag{11}$$

where N_i is the set of compartment numbers that joint compartment i (for our one-dimensional case, N_i will have two members), U_{ij} and A_{ij} are the averaged velocity and cross-sectional area between compartments i and j, and n_{ij} is the directional sign from compartment i to compartment j. If it is along the positive direction from compartment i to compartment j, $n_{ij}=1$. On the other hand, if it is along the negative direction, $n_{ij}=-1$. Consequently $n_{ij}=-n_{ji}$.

Similarly applying the ICM method to equation (2), we obtain for the discrete value Q_i at compartment i:

$$\frac{dQ_i}{dt}\Delta x_i = -\sum_{j\in N_i}(n_{ij}\,.\,U_{ij})Q_{ij} - gA_i\sum_{j\in N_i}n_{ij}h_{ij} - gA_i\sum_{j\in N_i}n_{ij}z_{0ij} + \frac{\Delta x_i m_i}{\rho} + \frac{\Delta x_i}{\rho}(\tau_i^{w}B_i - \tau_i^{b}P_i) + 2\nu_T\sum_{j\in N_i}\frac{(Q_j-Q_i)}{(\Delta x_i+\Delta x_j)} \tag{12}$$

In equations (11) and (12), A_{ij} and Q_{ij} must be interpolated in terms of their nodal values (A_i, A_j and Q_i, Q_j) to close the system. In this paper, the following formulae are proposed.

$$A_{ij} = \theta\frac{(\Delta x_j A_i + \Delta x_i A_j)}{(\Delta x_i+\Delta x_j)} + 0{\cdot}5(1-\theta)[(1+\gamma)A_i + (1-\gamma)A_j] \tag{13}$$

and

$$Q_{ij} = \theta\frac{(\Delta x_j Q_i + \Delta x_j Q_i)}{(\Delta x_i+\Delta x_j)} + 0{\cdot}5(1-\theta)[(1+\gamma)Q_i + (1-\gamma)Q_j] \tag{14}$$

where θ is a number ranging from 0·0 to 1·0 and γ is given by:

$$\gamma = 1{\cdot}0 \quad \text{if} \quad (n_{ij} \,.\, U_{ij}) > 0 \tag{15a}$$

and

$$\gamma = -1{\cdot}0 \quad \text{if} \quad (n_{ij} \,.\, U_{ij}) < 0 \tag{15b}$$

The value of θ is determined by the time-integration scheme for equations (11) and (12). The value of θ is equal to 0·0 for the explicit scheme, 0·5 for the Crank–Nicholson central difference, and 1·0 for the implicit scheme.

Substituting equation (13)–(15b) into equations (11) and (12), we obtain the following system of ordinary differential equations for Q and A:

$$[\mathbf{M}]\left\{\frac{\mathrm{d}\mathbf{A}}{\mathrm{d}t}\right\} + [\mathbf{S}]\{\mathbf{A}\} = \{\mathbf{F}\} \tag{16}$$

and

$$[\mathbf{M}]\left\{\frac{\mathrm{d}\mathbf{Q}}{\mathrm{d}t}\right\} + [\mathbf{W}]\{\mathbf{Q}\} + [\mathbf{T}]\{\mathbf{h}\} = \{\mathbf{G}\} \tag{17}$$

where [**M**] is the global diagonal matrix given by

$$M_{ii} = \Delta x_i, \qquad I = 1, 2, 3, \ldots \tag{18a}$$

$$M_{ik} = 0, \qquad k \neq i \tag{18b}$$

{**F**} and {**G**} are the global column vectors given by

$$F_i = \Delta x_i q_i, \qquad i = 1, 2, 3, \ldots \tag{19}$$

and

$$G_i = \frac{\Delta x_i}{\rho}(\tau_i^{\mathrm{w}} B_i - \tau_i^{\mathrm{b}} P_i) - [\mathbf{T}]\{z_0\} + \frac{\Delta x_i m_i}{\rho}, \qquad i = 1, 2, \ldots \tag{20}$$

and [**S**], [**W**] and [**T**] are the global banded matrices. These banded matrices are obtained by assembling the link matrices, which are to be defined in the following paragraph.

Referring to Figure 4, the link i–j has as its end points global node numbers i and j, respectively. Let us denote i as node number 1 and j as node number 2 in the local numbering system. Then link matrices $[_l\mathbf{S}]$, $[_l\mathbf{W}]$, and $[_l\mathbf{T}]$ will each have four entries. These entries are obtained from equations (13) and (14) as follows:

$${}_lS_{11} = (n_{11} \,.\, U_{12})\{\theta[\Delta x_2/(\Delta x_1 + \Delta x_2)] + 0{\cdot}5(1-\theta)(1+\gamma)\} \tag{21a}$$

$${}_lS_{12} = (n_{12} \,.\, U_{12})\{\theta[\Delta x_1/(\Delta x_1 + \Delta x_2)] + 0{\cdot}5(1-\theta)(1-\gamma)\} \tag{21b}$$

$${}_lS_{21} = -{}_lS_{11}, \qquad {}_lS_{22} = -{}_lS_{12} \tag{21c}$$

$${}_lW_{11} = (n_{12} \,.\, U_{12})\{\theta[\Delta x_2/(\Delta x_1 + \Delta x_2)] + 0{\cdot}5(1-\theta)(1+\gamma)\} + 2\nu_{\mathrm{T}}/(\Delta x_1 + \Delta x_2) \tag{22a}$$

$${}_lW_{12} = (n_{12} \,.\, U_{12})\{\theta[\Delta x_1/(\Delta x_1 + \Delta x_2)] + 0{\cdot}5(1-\theta)(1-\gamma)\} - 2\nu_{\mathrm{T}}/(\Delta x_1 + \Delta x_2) \tag{22b}$$

$${}_lW_{21} = -{}_lW_{11}, \qquad {}_lW_{22} = -{}_lW_{12} \tag{22c}$$

and from linear interpolation of h_{ij}

$$_lT_{11} = gA_1 n_{12}\,\Delta x_2/(\Delta x_1 + \Delta x_2) \tag{23a}$$

$$_lT_{12} = gA_1 n_{12}\,\Delta x_1/(\Delta x_1 + \Delta x_2) \tag{23b}$$

$$_lT_{21} = gA_2 n_{21}\,\Delta x_2/(\Delta x_1 + \Delta x_2) \tag{23c}$$

$$_lT_{22} = gA_2 n_{21}\,\Delta x_1/(\Delta x_1 + \Delta x_2) \tag{23d}$$

In equations (21a)–(23d), the subscript l in the lower left-hand corner of variables denotes the links. It is noted that equation (21a), (21b), (22a), and (22b) result in upstream interpolation on advection terms in equations (11) and (12) if $\theta = 0{\cdot}0$, i.e. an explicit scheme. If an implicit scheme ($\theta = 1$) is used to solve the matrix system [equations (16) and (17)], then the linear interpolation is followed and better accuracy is achieved.

The assembling procedure of obtaining the global matrices from the link matrices is the same as that from element matrices in the finite element method. For example, the assembling of [**T**] from [$_l$**T**] is demonstrated as follows. For a given link, one will have a 2×2 link matrix, [$_l$**T**]. Each of the four entries in the matrix [$_l$**T**] will constitute a fraction of the corresponding entries in the matrix [**T**]. If the corresponding global nodal numbers to local nodal numbers 1 and 2 are $N1$ and $N2$, then the entries $_lT_{11}$, $_lT_{12}$, $_lT_{21}$, and $_lT_{22}$ of the link matrix [$_l$**T**] are a partial sum of the entries $T_{N1,N1}$, $T_{N1,N2}$, $T_{N2,N1}$, and $T_{N2,N2}$ of the global matrix [**T**]. However, in the ICM algorithm, [**T**] is normally a banded matrix. Hence, denoting the half bandwidth plus one by IB, one would store the above four entries in the locations $T_{N1,IB}$, $T_{N1,N2-N1+IB}$, $T_{N2,N1-N2+IB}$, and $T_{N2,IB}$. Thus the assembling procedure is quite simple. First, one should initiate all entries of the global matrix [**T**]. Then for each link, one simply adds each of its four entries, $_lT_{11}$, $_lT_{12}$, $_lT_{21}$, and $_lT_{22}$, to the corresponding locations, $T_{N1,IB}$, $T_{N1,N2-N1+IB}$, $T_{N2,N1-N2+IB}$, and $T_{N2,IB}$, of the global matrix.

It is thus seen that the link in the ICM is equivalent to the element in the FEM and the linking compartments (nodes) equivalent to the element vertices (nodes). The major differences between ICM and FEM are: (a) the link matrices are obtained by the simple interpolation of interfacial values in terms of its linking nodal values by equations (13) and (14) to yield equations (21a)–(23d), whereas the element matrices must be obtained by numerical integration of the basis functions and their derivatives over the element, (b) the size of a link matrix is always 2×2 no matter what the spatial dimension is in the ICM, whereas the size of an element matrix depends on the type of element used and on the spatial dimensionality in the FEM. Thus, the ICM has the advantages of the simple interpolation of finite differences to yield link matrices and of the automatic generation of the finite element method to form the global matrices.

Equations (16) and (17) form a system of non-linear ordinary differential equations, since the matrices [**W**] and [**T**] and the column vector {**G**} depend on the dependent variables {**A**} and {**Q**}.

The following equations are used to compute the boundary values of Q and A:

(i) For prescribed flow boundaries

$$Q_B = Q_g \tag{24}$$

where Q_g is a given function of time and boundary node.

(ii) For the prescribed cross-sectional area boundary:

$$A_B = A_g \tag{25}$$

(iii) For the prescribed rating curve boundary:

$$Q_B = f(A_B) \tag{26}$$

in which f is a function relating the flow rate to the cross-sectional area at the boundary node.

(iv) For a junction:

$$\frac{dV_J}{dt} = -\sum_{J \in N_I} Q_I \cdot n_{IJ} \tag{27a}$$

$$h_J = f_J^{-1}(V_j) \tag{27b}$$

In equations (24)–(27b), the subscript B denotes the value to be evaluated at the boundary, the subscript I represents the value at a compartment interfacing with the boundary or with the junction, the subscript J describes the value at the junction, and n_{IJ} is the directional sign from node I to node J.

By using the ICM method,[21] the original continuous problem [equations (1) and (2) subject to equations (6)–(10)] is reduced to a system of ordinary differential equations in time [equations (16) and (17) subject to equations (24)–(27b)]. To complete the model, an effective technique must be developed to advance the solution in time from a given initial condition. The choice of scheme depends on required features of accuracy, stability, program ability, and computational efficiency. A thorough discussion of the time-integration schemes has been made elsewhere on the system of equations derived by finite difference methods[32–34] and by finite element methods.[35] Among the most commonly used schemes are (i) Euler's method, (ii) the trapezoidal rule, (iii) the improved trapezoidal rule, (iv) the iterative predictor–corrector method, (v) the Runge–Kutta methods, (vi) the time split method and (vii) the implicit method.

For the present study, the time split scheme will be used because it offers advantages in computer storage, computational efficiency, and a good degree of accuracy. Two options are provided: one is the time split implicit scheme and the other is the time split explicit scheme.

According to the time split implicit scheme, the advancement of $\{\mathbf{A}\}$ and $\{\mathbf{Q}\}$ from time $t^{(n)}$ to time $t^{(n+1)}$ is accomplished through two calculation cycles. In the first calculational cycle, the field of $\{\mathbf{A}^{(n+1)}\}$ is obtained by solving the following simultaneous equations:

$$([\mathbf{M}] + \Delta t[\mathbf{S}])\{\mathbf{A}^{(n+1)}\} = [\mathbf{M}]\{\mathbf{A}^{(n)}\} + \Delta t\{\mathbf{F}\} \tag{28}$$

and in the second calculational cycle, the field $\{\mathbf{Q}^{(n+1)}\}$ is obtained by solving the following matrix equation:

$$([\mathbf{M}] + \Delta t[\mathbf{W}])\{\mathbf{Q}^{(n+1)}\} = [\mathbf{M}]\{\mathbf{Q}^{(n)}\} - (\Delta t[\mathbf{T}]\{\mathbf{h}^{(n+1)}\} - \{\mathbf{G}\}) \tag{29}$$

It should be noted that in evaluating the matrix $[\mathbf{W}]$, the flow rates at the old time and cross-sectional area at the new time are used.

When the option of the time split explicit scheme is used, the advancement of $\{\mathbf{A}\}$ and $\{\mathbf{Q}\}$ from time $t^{(n)}$ to time $t^{(n+1)}$ is accomplished also through two calculational cycles. However, in the first cycle, equation (16) is used to compute the cross-sectional area field $\{\mathbf{A}^{(n+1)}\}$ as:

$$A_i^{(n+1)} = A_i^{(n)} - \frac{\Delta t}{M_{ii}}\left(\sum_{k=1} S_{ik} A_{ik}^{(n)} - F_i\right), \qquad i = 1, 2, \ldots \tag{30}$$

where $A_i^{(n+1)}$ is the value of A_i evaluated at time $(n+1)\,\Delta t$ and Δt is the time step size. In the second cycle, equation (17) is used to compute the new flow field $\{\mathbf{Q}^{(n+1)}\}$ based on the

newly obtained $\{\mathbf{A}^{(n+1)}\}$ and the old $\{\mathbf{Q}^{(n)}\}$ as follows:

$$Q_i^{(n+1)} = Q_i^{(n)} - \frac{\Delta t}{M_{ii}} \left(\sum_{+k} W_{ik} Q_k^{(n)} + \sum_{+k} T_{ik} h_k^{(n+1)} - G_i \right) \quad \text{for} \quad i = 1, 2, 3, \ldots . \tag{31}$$

It can be shown that the time split implicit scheme would yield an unconditionally linear stable solution. Thus, time step size can be very large, albeit dictated by the accuracy requirement and non-linear instability, which is very difficult to assess. On the other hand, the time step size for the time split explicit scheme will be limited by the Courant–Friedreichs–Lewy condition.[24] Nevertheless, this optional scheme is included because it offers advantages in computer storage requirement.

APPLICATIONS

Applications of the present model to a river network are demonstrated by two sample problems: a single river system and a network consisting of five river reaches. The validation of the model is a subject of future research. This paper deals mainly with the development and demonstration of the model. These two sample cases typify real-world problems.

A single river problem

To test the internal consistency of the computer code, a single river, 98 km long, is used (Figure 5). The width of the river is assumed to be 200 m and the bottom lies on a horizontal

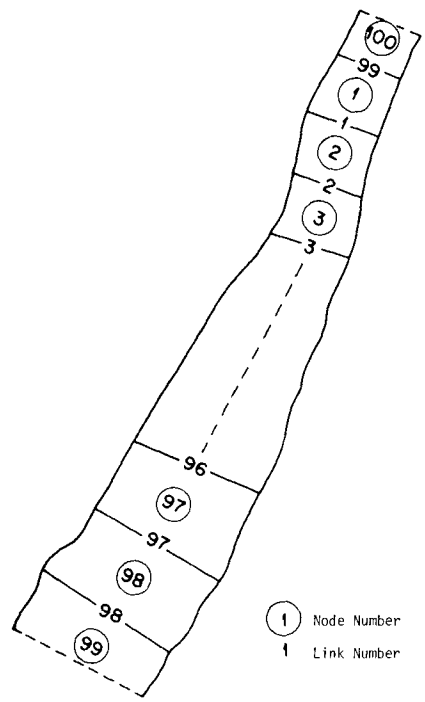

Figure 5. Single-channel discretization

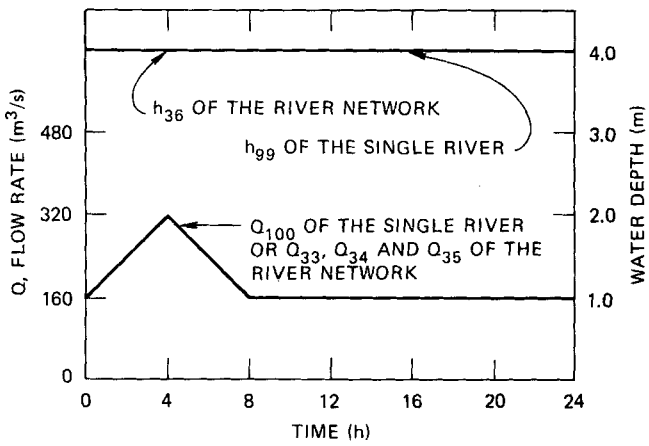

Figure 6. Boundary conditions for both the single river and river network problem

plane. The river is assumed to have a Manning coefficient of 0·03 in equation (4c) for the computation of stress exerted on the wet perimeter. The wind is assumed to be calm to yield $\tau^w = 0{\cdot}0$. To perform the ICM computation, the river is divided into 100 compartments as shown in Figure 5. Compartment numbers 1–98 are the interior nodes. Compartment number 100 is a boundary node with a prescribed flow rate as function of time (Figure 6), and compartment number 99 is a boundary node with a prescribed water depth of 4 m. Both the prescribed flow and depth can be functions of time. The initial conditions are obtained by solving the steady-state version of equations (16) and (17) using the same computer program with upstream inflow of 160 m^3/s and downstream water depth of 4 m. The simulation starts at time = 0 h and ends at time = 24 h with a time step size of 60 s. Figure 7 shows the simulated flows at node numbers 10, 30, 49, 75, and 99. The results confirm what one would expect. The peak flows further downstream are smaller than those at upstream nodes. The lag time of peak flows is longer the further downstream the node is. After reaching the peak, hydrographs at all five locations decrease asymptotically to the constant steady-state rate of 160 m^3/s.

A river network problem

One of the advantages of this model is its ability to deal with the river network that may consist of any number of joined and branched rivers/streams. To illustrate this point, a river network consisting of five river branches with two junctions is used (Figure 8). For the model simulation, the whole river network is divided into 36 compartments, three of which (compartment numbers 33, 34, and 35) are the prescribed-flow-boundary compartments. Compartment number 36 is a prescribed-depth-boundary compartment. Compartment numbers 14 and 25 are junction compartments. These compartments are joined by 35 links. The prescribed flow rates at compartments 33, 34, and 35 as a function of time and the prescribed water depth at compartment 36 are shown graphically in Figure 6. The initial conditions are once again obtained by solving the steady-state version of equations (16) and (17) with the invariant flow rate of 160 m^3/s imposed at compartments 33, 34, and 35, and the constant water depth of 4 m at compartment 36. The steady-state hydrodynamic variables obtained by using these time-invariant boundary conditions are given in Table I. Examining this Table, one gains confidence in the consistency of the computer code, as the

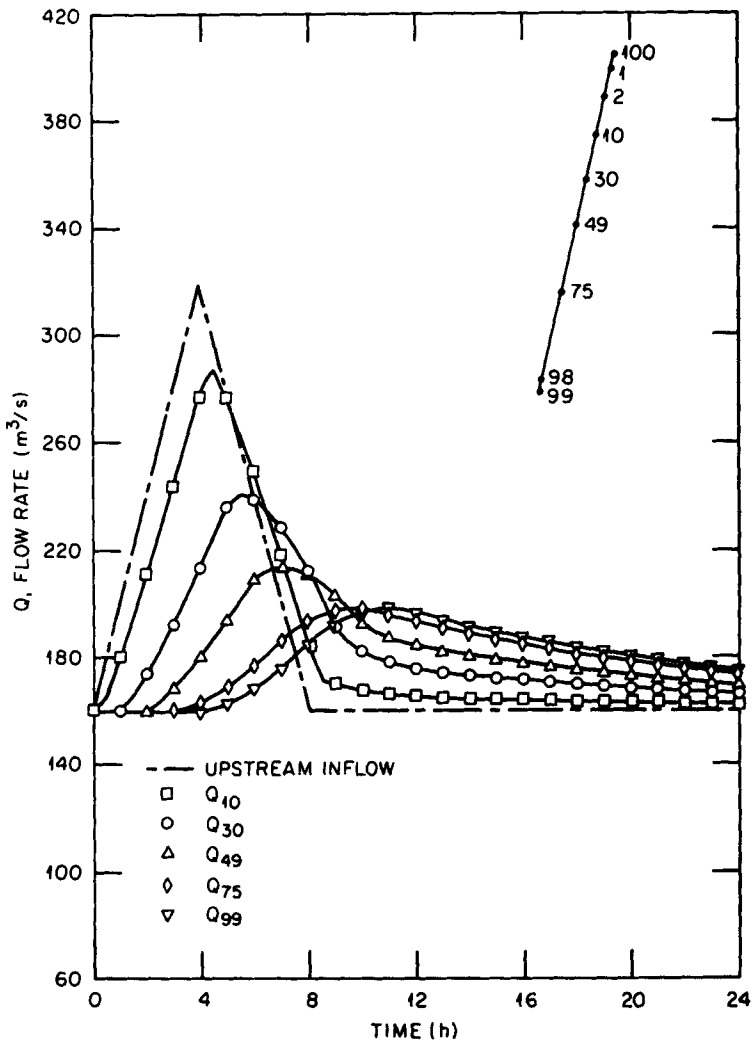

Figure 7. Hydrographs at nodes 10, 30, 49, 75, and 99 for the single river problem

water surface elevations at nodes 8, 7, 6, 5, and 4 are, respectively, equal to those at their corresponding nodes 13, 12, 11, 10, and 9 from the junction node 14 as expected. Furthermore, the elevations at nodes 18, 17, 16, and 15 are, respectively, greater than those at their corresponding nodes 23, 22, 21, and 20 from the junction node 25 because the flow rates at the former nodes are twice as large as those at the latter nodes.

Using the transiet boundary conditions of Figure 6, Figure 9 shows the resulting flow rate at nodes 8, 13, 15, 19, 24, 26, and 32. It is noted that the hydrograph at node 15 is almost equal to the sum of those at nodes 8 and 13 because the storage effect of the junction node 14 is small. Similarly, the hydrograph at node 26 is approximately equal to the sum of those at nodes 19 and 24. In contrast to the single river problem where the peak flows at downstream nodes are less than those at the upstream nodes, in this network system the peak flows at the downstream nodes are not necessarily smaller than those at the upstream nodes. For example, whereas the peak flow at node 19 is negligibly smaller than that at node

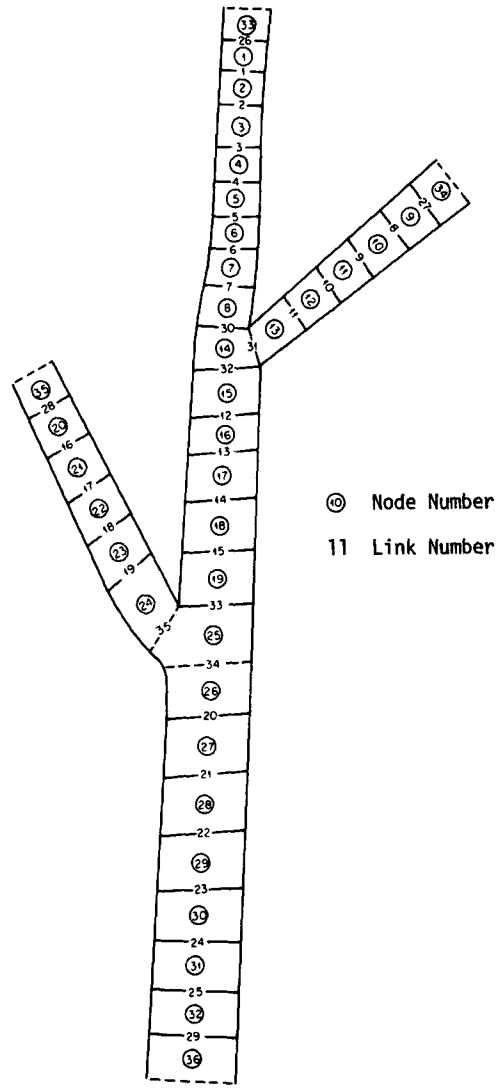

Figure 8. Channel network discretization

15, the peak flow at node 26 is much larger than that at node 15 because of the addition of flow from node 24.

Because no analytical solutions are available for the simultaneous system of equations (1)–(10), it is not possible to assess the accuracy of the results presented in both examples by comparing them with those of analytical results. The only confidence one has here is that these results behave qualitatively as one would intuitively expect. The ultimate judgement of the model will have to be made by comparing the simulations with laboratory experiments and field data. Because the main purpose of this paper is to document the construction of the model, the validation will have to be deferred to later studies.

Table I. Steady state hydrodynamic variables for the river network problem.

Node	Variables	Q $m^3 s^{-1}$	A m^2	h m	B m	P m
1		160·0	881·5	4·407	200·0	208·8
2		160·0	880·6	4·403	200·0	208·8
3		160·0	879·7	4·399	200·0	208·8
4		160·0	878·8	4·394	200·0	208·8
5		160·0	878·0	4·390	200·0	208·8
6		160·0	877·1	4·385	200·0	208·8
7		160·0	876·2	4·381	200·0	208·8
8		160·0	857·3	4·377	200·0	208·8
9		160·0	878·8	4·394	200·0	208·8
10		160·0	878·0	4·390	200·0	208·8
11		160·0	877·1	4385	200·0	208·8
12		160·0	876·2	4·381	200·0	208·8
13		160·0	875·3	4·377	200·0	208·8
14		320.0	175100	4·377	40000	43500
15		320·0	875·3	4·376	200·0	208·8
16		320·0	871·7	4·359	200·0	208·7
17		320·0	868·1	4·341	200·0	208·7
18		320·0	864·5	4·322	200·0	208·6
19		320·0	860·8	4·304	200·0	208·6
20		160·0	864·5	4·323	200·0	208·6
21		160·0	863·6	4·318	200·0	208·6
22		160·0	862·7	4·313	200·0	208·6
23		160·0	861·7	4·309	200·0	208·6
24		160·0	860·8	4·304	200·0	208·6
25		480·0	172200	4·304	40000	43440
26		480·0	860·8	4·304	200·0	208·6
27		480·0	852·3	4·262	200·0	208·5
28		480·0	843·6	4·218	200·0	208·4
29		480·0	834·9	4·173	200·0	208·3
30		480·0	825·2	4·126	200·0	208·3
31		480·0	815·5	4·077	200·0	208·2
32		480·0	805·4	4·027	200·0	208·1
33		160·0	881·5	4·407	200·0	208·8
34		160·0	878·8	4·394	200·0	208·8
35		160·0	864·5	4·323	200·0	208·6
36		480·0	800·0	4·000	200·0	208·0

Note: For junction nodes, A is the compartment volume (m^3); B is the surface area of the compartment, (m^2); and P is the wet area, (m^2).

CONCLUSION

A dynamic model for simulating the water depth and flow rate for stream/river networks has been developed. The usefulness of the model is demonstrated by applying it to two cases. The first one is to a single river problem to check the consistency of the computational algorithm and computer code. The second case is to a river network consisting of five river branches of comparative size. These applications yield qualitative results that one would expect. Quantitative verifications require further studies.

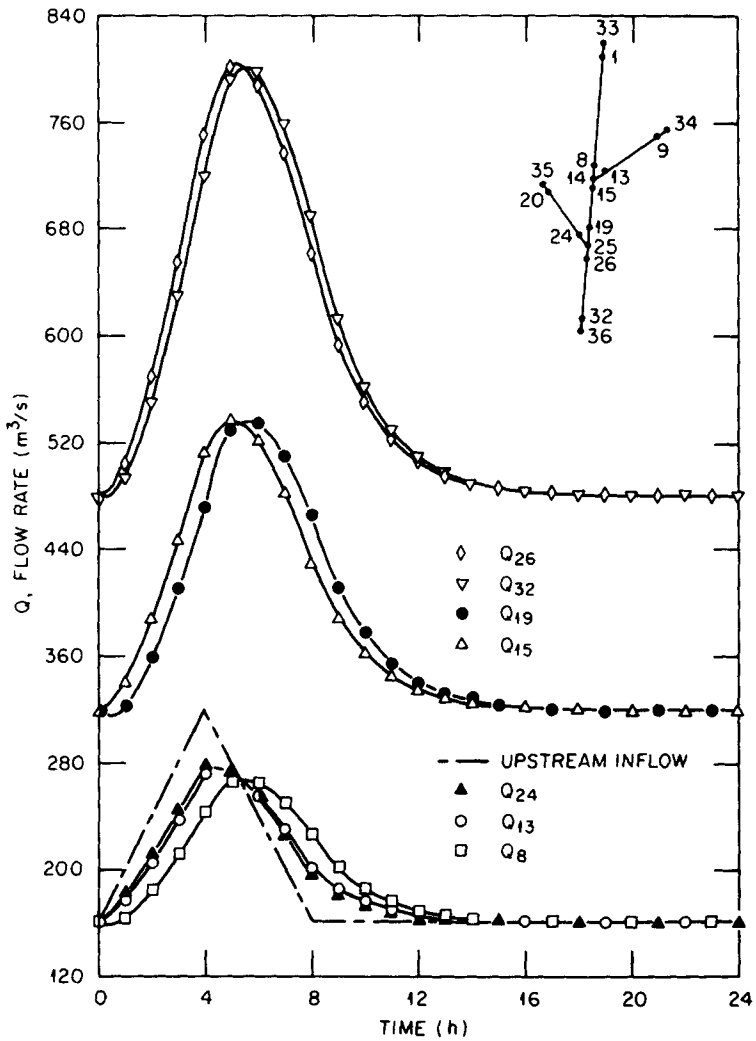

Figure 9. Hydrographs at nodes 8, 13, 15, 19, 24, 32, and 36 for the river network problem

ACKNOWLEDGMENTS

This research was sponsored by the Office of Pesticide and Toxic Substances, U.S. Environmental Protection Agency under Interagency Agreement No. EPA-AD-89-F-1-399-0 and with the U.S. Department of Energy under contract W-7405-eng-26 with Union Carbide Corporation. Publication No. 2185, Environmental Sciences Division, ORNL.

REFERENCES

1. G. T. Yeh, *CHNTRN: A CHaNnel TRaNsport Model for Simulating Sediment and Chemical Transport in a Stream/River Network*, ORNL-5882, *Oak Ridge National Laboratory, Oak Ridge, Tennessee*, 1982.
2. A. S. Donigian, Jr., D. C. Beyerlein, H. H. Davis, Jr. and N. H. Crawford, *Agricultural Runoff Mangement (ARM) Model Version II: Refinement and Testing*. EPA-600/3-77-098, Office of Research and Development, Environmental Research Laboratory, U. S. EPA, Athens, Geogia, 294 pp., 1977.

3. R. M. Li, D. B. Simons and M. A. Stevens, 'Nonlinear kinematic wave approximation for water routing', *Water Resources Research*, **11,** (2), 245–252 (1975).
4. K. M. Leytham and R. C. Johanson, *Watershed Erosion and Sediment Transport Model*, EPA-600/3-79-028, Office of Research and Development, Environmental Research Laboratory, U. S. EPA, Athens, Geogia, 357 pp., 1979.
5. M. B. Abbott, *Computational Hydraulics*, Pitman, London, 1979.
6. J. A. Cunge, F. F. Holly, Jr. and A. Verway, *Practical Aspects of Computational River Hydraulics*, University of Colorado, Ford Collins, Colorado, 1980.
7. M. Amein and H. L. Chu, 'Implicit numerical modeling of unsteady flows', *J. Hydraulic Dvision, ASCE*, **101,** (HY6), 717–751 (1975).
8. D. L. Fread, 'Technique for implicit dynamic routing in rivers with tributaries', *Water Resources Research*, **9,** (4), 918–926 (1973).
9. D. R. F. Harleman and C. H. Lee, 'The computation of tides and currents in estuaries and canals', *Technical Bulletin No.* 16, Hydrodynamic Laboratory, Massachusetts Institute of Technology, Cambridge, Mass., 143 pp., 1969.
10. J. W. Kaumphis, 'Mathematical tidal study of St. Lawrence River', *J. Hydraulic Division, ASCE* **96,** (HY3), 643–644 (1970).
11. C. Lai, 'Computation of transient flows in rivers and estuaries by multiple-reach method of characteristics', *Professional Paper* 575-*D*, U.S.G.S., Reston, Virgina, 1967.
12. J. A. Liggett, and D. A. Woolhiser, 'Difference solutions of the shallow-water equation', *J. Eng. Mech., ASCE*, **93,** (ME2), 40–71 (1967).
13. F. H. Quinn, and E. B. Wylie, 'Transient analysis of the Detroit river by the implicit method', *Water Resources Research*, **8,** (6), 1461–1469 (1972).
14. A. O. Akan and B. C. Yen, 'Diffusion-wave flood routing in channel networks', *J. Hydraulic Division, ASCE*, **107,** (HY6), 719–732 (1981).
15. J. P. Bennett, 'General model to simulate flow in branched estuaries', *Proc. Symp. on Modeling Technique, ASCE*, 643–662 (1975).
16. D. L. Fread, *National Weather Service Operational Dynamic Wave Model* (*DWOPER*), National Weather Service, NOAA, Silver Spring, Md., 1978.
17. R. W. Scheffranck, R. A. Baltzer and D. E. Goldberg, *A Model for Simulation of Flow in Singular and Interconnected Channels*, Book 7, Chapter C3, Techniques for Water-Resources Investigations of the United States Geological Survey, U.S. Government Print Office, Washington, D.C.
18. E. F. Wood, B. M. Harley, and F. E. Perkins, 'Operations characteristics of a numerical solution for the simulation of open channel flow', *Hydrodynamic Lab. Report No.* 150, Dept. of Civil Engineering, MIT, Cambridge, Mass., 1972.
19. E. F. Wood, B. M. Harley, and F. E. Perkins, 'Transient flow routing in channel networks', *Water Resources Research*, **11,** (3), 423–430 (1975).
20. Barre de Saint-Venant, 'Theory of unsteady water flow with application to river floods and propagation of tides in river channels', *Acad. Sci. (Paris) Comptes Rendus*, **73,** 237–240 (1871).
21. G. T. Yeh, 'Numerical solutions of Navier–Stokes equations with an integrated compartment (ICM)', *Int. j. numer. methods fluids*, **1,** 207–223 (1981).
22. T. N. Narasimhan and P. A. Witherspoon, 'An integrated finite difference method for analyzing fluid flow in porous media', *Water Resources Research*, **12,** 56–67 (1967).
23. F. M. Henderson, *Open Channel Flow*, MacMillan, New York, 522 pp., 1966.
24. G. T. Yeh, *CHNTRN: A CHaNnel TRaNsport Model for Simulating Sediment and Chemical Fates in a Stream/River Network*, ORNL-5882, Oak Ridge National Laboratory, Oak Ridge, Tennessee, 1982.
25. H. Schlichting, *Boundary Layer Theory*, McGraw-Hill, New York, 747 pp., 1968.
26. J. W. Daily, and D. R. F. Harleman, *Fluid Dynamics*, Addision-Wesley, Reading, Massachusetts, 454 pp., 1966.
27. V. T. Chow, *Handbook of Applied Hydrology*, Chapter 7, McGraw-Hill, New York, 1964.
28. K. L. Denman, and M. Miyake, 'Behavior of the mean wind, the drag coefficient, and the wave field in the open ocean', *Geophys. Res.* **78,** (12) 1917–1931 (1973).
29. W. Van Dorn, Wind stress on an artificial pond, *J. Mar. Res.* **12,** (3), 349–276 (1953).
30. J. Wu, Wind stress and surface roughness at air–sea interface, *J. Geophys. Res.*, **74,** (2), 444–455 (1969).
31. N. S. Heaps, A two-dimensional numerical sea model, *Philos. Trans. R. Soc. London Ser. A*, **265,** (1160), 93–137 (1969).
32. R. D. Richtmeyer, and K. W. Morton, *Difference Methods for Initial Value Problems*, Interscience, New York, 238 pp., 1967.
33. P. J. Roache, *Computational Fluid Dynamics*, Hermosa, Albuquerque, New Mexico, 446 pp., 1972.
34. J. J. Leendertse, 'Aspects of a computational model for long-period water-wave propagation', *Memorandum Rm*-5294-*PR*, Rand Corporation, Santa Monica, California, 165 pp., 1967.
35. J. D. Wang, and J. J. Connor, 'Mathematical modeling of near coastal circulation', *Report No. MITSG* 175–13, Massachusetts Institute of Technology, Cambridge, Mass., 272 pp., 1975.